Behavior of oxygen vacancies in single-crystal $SrTiO_3$: Equilibrium distribution and diffusion kinetics

Roger A. De Souza* and Veronika Metlenko
Institute of Physical Chemistry, RWTH Aachen University, D-52056 Aachen, Germany

Daesung Park and Thomas E. Weirich
GFE - Central Facility for Electron Miscroscopy, RWTH Aachen University, Ahornstrasse 55, 52074 Aachen, Germany

(Received 16 March 2012; published 24 May 2012)

$^{18}O/^{16}O$ exchange and subsequent time-of-flight secondary ion mass spectrometry (ToF-SIMS) analysis was employed to investigate the transport of oxygen, and thus the behavior of oxygen vacancies, in [nominally undoped, (100) oriented] single-crystal $SrTiO_3$ substrates. Isotope exchange anneals were performed as a function of temperature, $948 < T/\mathrm{K} < 1123$, at an oxygen activity $aO_2 = 0.50$ and as a function of oxygen activity, $0.01 < aO_2 < 0.70$, at $T = 1073$ K. All isotope profiles show the same characteristic form: an initial drop over tens of nanometers close to the surface, which is attributed to an equilibrium space-charge layer depleted of oxygen vacancies, followed by a profile extending several microns into the solid, which is attributed to diffusion in a homogeneous bulk phase. The entire isotope profile can be described quantitatively by a numerical solution to the diffusion equation with a position-dependent diffusion coefficient; the description yields the tracer diffusion coefficient in the bulk $D^*(\infty)$, the surface exchange coefficient k_s^*, and the space-charge potential Φ_0. All $D^*(\infty)$ data are consistent with nominally undoped $SrTiO_3$ substrates being weakly acceptor doped; the activation enthalpy for the migration of oxygen vacancies in bulk $SrTiO_3$ is found to be $\Delta H_{\mathrm{mig,V}} \approx 0.6$ eV. The surface termination of the $SrTiO_3$ substrates was seen to affect significantly the surface exchange coefficient k_s^*. Values of Φ_0 obtained as a function of T and aO_2 are approximately 0.5 V, indicating strong depletion of oxygen vacancies within the equilibrium surface space-charge layers. Thermodynamic modeling indicates that space-charge formation at the TiO_2-terminated (100) surface is driven by the Gibbs formation energy of oxygen vacancies at the interface being lower than in the bulk.

DOI: 10.1103/PhysRevB.85.174109 PACS number(s): 66.30.hd, 73.30.+y, 61.72.−y, 68.35.Dv

I. INTRODUCTION

There is renewed interest in the behavior of point defects in the perovskite-type oxide strontium titanate, $SrTiO_3$. For decades point-defect behavior in $SrTiO_3$ was investigated primarily because of the material's ability to serve as a proxy: $SrTiO_3$ is not only a representative system for closely related, more complex perovskite-type oxides, such as $BaTiO_3$, $Pb(Zr,Ti)O_3$, and $MgSiO_3$, but also a model mixed ionic and electronic conductor.[1–8] Increasingly, point-defect behavior in $SrTiO_3$ is attracting attention in its own right because of the material's possible application as an active component in all-oxide electronics,[9–13] and as a memristive element.[14–16] In particular, the behavior of oxygen vacancies in the bulk $SrTiO_3$ phase and at its extended defects (dislocations, interfaces) has been implicated, to varying degrees, in determining the principal phenomenon, the performance or the reliability of such devices.[17–22]

One key method for probing the behavior of oxygen point defects in an oxide is to study the diffusion of oxygen. Indeed, oxygen diffusion in $SrTiO_3$ has been studied since the 1960s;[23–49] and from the earliest investigations there has been universal agreement that oxygen diffusion occurs by a vacancy mechanism. Yet, almost half a century later there is little consensus as to the migration enthalpy of these defects, $\Delta H_{\mathrm{mig,V}}$, with experimental values varying from 0.3 to 2.1 eV,[23–34,39–42] and theoretical values varying from 0.4 to 1.4 eV.[43–49] The first aim of this study is to use a well-established method for investigating oxygen transport in solids—$^{18}O/^{16}O$ isotope exchange and secondary ion mass spectrometry (SIMS) analysis[50–54]—to determine the activation enthalpy for vacancy migration in $SrTiO_3$. The combination of isotope exchange and SIMS has been applied in the past to $SrTiO_3$,[34,37,38] but not with the express aim of determining the vacancy diffusion coefficient D_V as a function of temperature, and subsequently, the vacancy migration enthalpy, $\Delta H_{\mathrm{mig,V}}$ [$D_V = D_V^0 \exp(-\Delta H_{\mathrm{mig,V}}/kT)$].

The second aim of this study concerns the equilibrium distribution of oxygen vacancies close to the (100) surface of single-crystal $SrTiO_3$ substrates. In the case of grain boundaries in acceptor-doped strontium titanate, it is well documented (see Refs. 55–58 and references therein) that these interfaces are enveloped in equilibrium space-charge layers that are strongly depleted of oxygen vacancies (and also of electron holes): it is this drastic reduction in point-defect concentrations that gives rise to the transport of charge and mass in acceptor-doped titanate polycrystals being severely hindered. In contrast, the effects of an equilibrium surface space-charge layer on $SrTiO_3$'s physical, chemical, and electrochemical properties are not well known. Part of the problem has been the lack of a suitable experimental technique with which to probe nonuniform point-defect concentrations at a gas-solid interface under thermodynamically well-defined conditions. Recently, studies of acceptor-doped $SrTiO_3$ (Refs. 37 and 59) and $Pb(Zr,Ti)O_3$ (Ref. 60) have demonstrated that an isotope exchange experiment with subsequent SIMS analysis provides an elegant, though indirect, method for spatially resolving the distribution of point defects in an equilibrium surface space-charge layer. In this study we aim, by performing isotope

 ©2012 American Physical Society

exchange experiments as a function of temperature and oxygen partial pressure, not only to characterize the behavior of the space-charge potential at the (100) surface of $SrTiO_3$, but also to elucidate its origin.

II. THEORY

We focus on acceptor-doped $SrTiO_3$ because chemical analyses indicated that the (nominally undoped) single-crystal samples we studied contained small amounts of Al as an acceptor impurity (see Sec. III). The experimental data obtained for the bulk tracer diffusion coefficient are also consistent with the samples being weakly acceptor doped (see Sec. V).

A. Bulk defect chemistry

The defect chemistry of $SrTiO_3$ doped with a fixed valence acceptor is governed under dry conditions by three reactions[1–8] (c_{def} is the concentration of defect def; aX is the activity of component X and is numerically equal to the partial pressure of X in bar):

(1) the generation of electrons and holes by thermal excitation across the band gap,

$$\text{null} \rightleftharpoons \text{e}' + \text{h}^{\cdot}, \tag{1}$$

with equilibrium constant,

$$K_{\text{eh}}(T) = c_{\text{e}'}\, c_{\text{h}^{\cdot}}; \tag{2}$$

(2) SrO-partial Schottky disorder,

$$\text{Sr}_{\text{Sr}}^{\times} + \text{O}_{\text{O}}^{\times} \rightleftharpoons \text{V}_{\text{Sr}}'' + \text{V}_{\text{O}}^{\cdot\cdot} + \text{SrO}(g), \tag{3}$$

with equilibrium constant,

$$K_{\text{Sch}}(T) = c_{\text{V}_{\text{Sr}}''}\, c_{\text{V}_{\text{O}}^{\cdot\cdot}}\, a\text{SrO}; \tag{4}$$

(3) reduction of the oxide to create oxygen vacancies and electrons,

$$\text{O}_{\text{O}}^{\times} \rightleftharpoons \tfrac{1}{2}\text{O}_2(g) + \text{V}_{\text{O}}^{\cdot\cdot} + 2\text{e}', \tag{5}$$

with equilibrium constant

$$K_{\text{Red}}(T) = (a\text{O}_2)^{1/2} c_{\text{V}_{\text{O}}^{\cdot\cdot}} (c_{\text{e}'})^2. \tag{6}$$

Various sets of numerical parameters for the equilibrium constants $K_{\text{eh}}(T)$, $K_{\text{Sch}}(T)$, and $K_{\text{Red}}(T)$ are given in the literature.[5,6,41]

To maintain charge neutrality within the bulk phase, the concentrations of point defects must satisfy

$$c_{\text{e}'} + c_{\text{Acc}'} + 2c_{\text{V}_{\text{Sr}}''} = c_{\text{h}^{\cdot}} + 2c_{\text{V}_{\text{O}}^{\cdot\cdot}}, \tag{7}$$

where the concentration of acceptor impurities is predominantly given by Al residing on Ti sites. Combining Eqs. (2), (4), (6), and (7) allows all point defect concentrations to be predicted as a function of T, $a\text{O}_2$, $a\text{SrO}$, and acceptor dopant concentration.

Since cation diffusion only becomes appreciable at much higher temperatures than those used in this study,[61,62] however, the concentration of cation vacancies in the bulk phase may be assumed to be frozen in from higher temperatures. As a consequence cation vacancies may be regarded effectively as additional acceptors and $a\text{SrO}$ is no longer a variable that needs to be considered. Thus Eq. (7) may be approximated (for not too high temperatures and not extremely reducing conditions) by

$$c_{\text{Acc}'} \approx 2c_{\text{V}_{\text{O}}^{\cdot\cdot}} > c_{\text{h}^{\cdot}} \gg c_{\text{e}'}, \tag{8}$$

i.e., the acceptor-dopant species (impurity acceptors and frozen-in cation vacancies) are compensated by oxygen vacancies.

B. Probing inhomogeneous point-defect distributions close to an interface

The current diffusion problem—isotope transport across a gas-solid interface, through a space-charge layer depleted of oxygen vacancies, and into a bulk phase of uniform vacancy concentration—was treated within the framework of linear irreversible thermodynamics in a previous paper.[59] Here a brief summary of the procedure for obtaining the entire oxygen isotope profile in the solid is given. This procedure, which approximates the solid as a one-dimensional continuum, consists of two steps. The first step is to calculate the equilibrium distribution of oxygen vacancies within the space-charge layer,

$$c_{\text{V}_{\text{O}}^{\cdot\cdot}}(x) = c_{\text{V}_{\text{O}}^{\cdot\cdot}}(\infty) e^{-2e\phi(x)/kT}, \tag{9}$$

where $\phi(x)$, the electrical potential, is obtained by solving the appropriate Poisson-Boltzmann equation. In the present case, it is assumed that the acceptor dopant is immobile, and thus that its concentration in the space-charge layer is constant (Mott-Schottky case).[63,64] The appropriate Poisson-Boltzmann equation is thus

$$\varepsilon_0\varepsilon_{\text{r}}\frac{d^2\phi}{dx^2} = -\rho = e\big[c_{\text{Acc}'} - 2c_{\text{V}_{\text{O}}^{\cdot\cdot}}(\infty)e^{-2e\phi(x)/kT} - c_{\text{h}^{\cdot}}(\infty)e^{-e\phi(x)/kT} + c_{\text{e}'}(\infty)e^{+e\phi(x)/kT}\big], \tag{10}$$

where $\varepsilon_0\varepsilon_{\text{r}}$ is the dielectric permittivity and ρ is the space-charge density. The two boundary conditions used for solution are $\Phi_0 = \phi(\infty) - \phi(0)$ and $\nabla\phi(\infty) = 0$; $x = \infty$ refers to a position far away from the space-charge layer in the electroneutral bulk phase. Φ_0 is the space-charge potential and takes positive values, so that in the space-charge layer the positively charged vacancies are depleted. The origin of positive Φ_0 is discussed in Sec. V B.

From the oxygen vacancy distribution across the sample, the variation in the local tracer diffusion coefficient across the sample follows as (f^* is the tracer correlation factor)

$$D^*(x) = f^* D_{\text{V}} \frac{c_{\text{V}_{\text{O}}^{\cdot\cdot}}(x)}{c_{\text{O}_{\text{O}}^{\times}}(x)} \approx D^*(\infty)e^{-2e\phi(x)/kT}. \tag{11}$$

Thus, because oxygen vacancies are depleted in the space-charge layer, $D^*(x)$ is strongly diminished towards the surface [see Fig. 1(a)].

The second step to obtaining the isotope profile in the solid is to solve Fick's second law for the isotope fraction n^*,

$$\frac{\partial n^*}{\partial t} = \frac{\partial}{\partial x}\left[D^*(x)\frac{\partial n^*}{\partial x}\right], \tag{12}$$

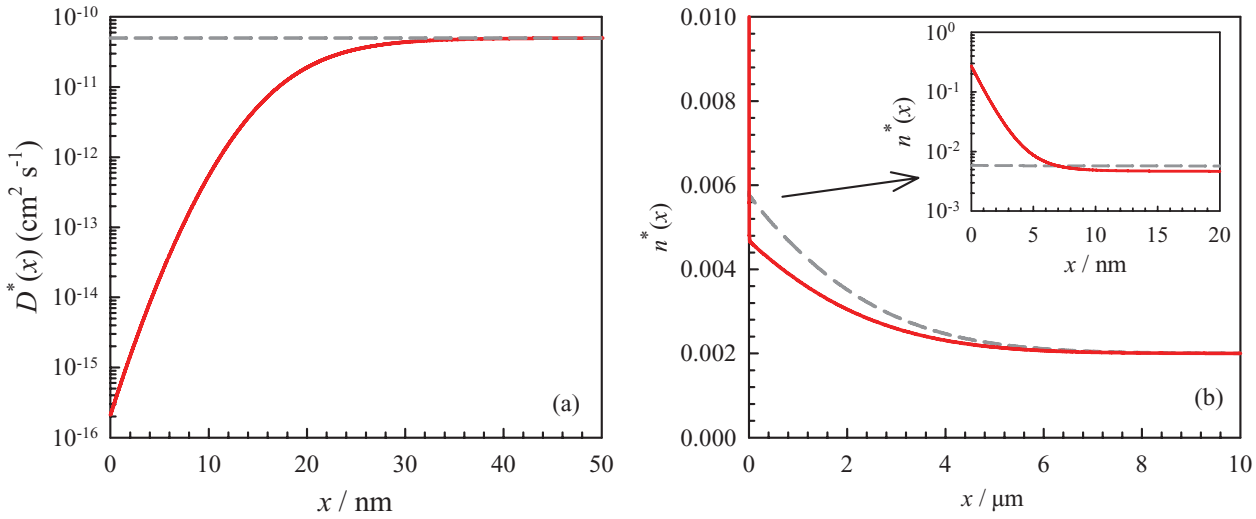

FIG. 1. (Color online) Effect of an equilibrium space-charge layer depleted of oxygen vacancies on oxygen isotope transport. (a) Local tracer diffusion coefficient $D^*(x)$. (b) Isotope fraction in the solid, $n^*(x)$. Inset shows the additional profile in the space-charge layer. Red solid lines: with space-charge layer; grey dashed lines: without space-charge layer. Calculations performed for $c_{\mathrm{Acc}'} = 10^{25}$ m^{-3}, $T = 750$ K, $\varepsilon_r = 125$, $\Phi_0 = 0.4$ V, $k_s^* = 7.5 \times 10^{-10}$ cm s^{-1}, $D^*(\infty) = 5 \times 10^{-11}$ cm^2 s^{-1}, $t = 10^3$ s.

with $D^*(x)$ given by Eq. (11). The appropriate initial and boundary conditions correspond to isotope exchange between a large volume of gas and a semi-infinite medium with limited surface kinetics:

$$n^*(x \geqslant 0, t = 0) = n_{\mathrm{bg}}^*, \tag{13a}$$

$$n^*(x = \infty, t \geqslant 0) = n_{\mathrm{bg}}^*, \tag{13b}$$

$$k_s^*[n_g^* - n^*(x = 0, t)] = -D^*(x = 0)\left.\frac{\partial n^*}{\partial x}\right|_{x=0}. \tag{13c}$$

n_g^* is the isotope fraction of the annealing gas; n_{bg}^* is the background isotope fraction. Both partial differential equations (first, Poisson-Boltzmann; second, Fick's second law) were solved numerically with the finite element package COMSOL (COMSOL AB, Stockholm, Sweden), as no analytical solutions are available. An example result is plotted in Fig. 1(b): the region of locally reduced diffusivity, arising from the surface space-charge layer, is seen to give rise to an additional isotope profile close to the surface. It is emphasized that (i) the extent of the additional profile is always smaller than the extent of the space-charge zone because large deviations of $D^*(x)$ from the bulk value are required to produce a noticeable additional profile,[59] and (ii) this additional profile cannot be described by a simple exponential, Gaussian, or error function.

It is also noted that the profile in the bulk phase (i.e., excluding the additional profile within the space-charge zone) is described exactly by the analytical solution to the diffusion equation for the initial and boundary conditions given in Eq. (13) with bulk tracer diffusion $D^*(\infty)$ and an effective surface exchange coefficient k_{eff}^*, which is a function of k_s^* and Φ_0. In terms of the dimensionless parameters $x' = x/\sqrt{4D^*(\infty)t}$ and $h' = k_{\mathrm{eff}}^*\sqrt{t/D^*(\infty)}$, the analytical solution is[65]

$$n^*(x,t) = n_{\mathrm{bg}}^* + (n_g^* - n_{\mathrm{bg}}^*)\mathrm{erfc}(x') - \exp(h'x' + h'^2)\cdot\mathrm{erfc}(x' + h'). \tag{14}$$

III. EXPERIMENT

A. Sample preparation and characterization

Single-crystal samples of nominally undoped and (100) oriented $SrTiO_3$, measuring 10 mm × 10 mm × 1 mm and polished on one large face, were obtained commercially from CrysTec GmbH (Berlin, Germany). All samples were cut from the same boule, so that the type and concentration of impurities would not vary from sample to sample. Chemical analysis (and SIMS) indicated that the predominant impurity in these single crystals was Al (with small amounts of Mg). These species are expected to substitute for Ti and thus to act as acceptor dopants; the effective concentration of acceptors (including frozen-in cation vacancies) is estimated to be 7×10^{17} cm^{-3}.

The as-received $SrTiO_3$ single-crystal samples were first annealed at $T = 1273$ K in air for 24 h, in order to remove polishing damage. They were subsequently cleaned with acetone, isopropanol and demineralized water (in that order), treated with buffered HF solution (NH_4F:HF with a pH = 4.5), and then annealed at $T = 1223$ K for 2 h in air, in order to produce TiO_2-terminated surfaces.[66,67]

Atomic force micrographs (AFMs) of the substrates' surface, after the second anneal at $T = 1223$ K, were acquired with an ULTRA Objective PICO station (Surface Imaging Systems, Herzogenrath, Germany). Measurements were performed in noncontact mode.

Samples for analysis by transmission electron microscopy (TEM) were prepared on an FEI Strata 205 Focussed Ion Beam (FIB) workstation (FEI, Eindhoven, Netherlands). High resolution transmission electron microscopy (HRTEM) images were obtained with a Tecnai F20 microscope (FEI, Eindhoven, Netherlands) operated at 200 kV.

B. Isotope exchange experiments/ToF-SIMS analysis

The standard procedure for introducing an isotope penetration profile into a solid from a large volume of gas was

employed.[50–52] A sample was first equilibrated for a time t_{eq} ($t_{eq} \geqslant 10t$) at the temperature and oxygen partial pressure of interest in oxygen of natural isotopic abundance, and then quenched to room temperature. It was subsequently given an anneal for a time t, in highly enriched $^{18}O_2$ gas (Isotec Inc., Miamisburg, USA) at the same temperature and oxygen partial pressure. The ^{18}O isotope fractions in the annealing gases were determined prior to the exchange experiments by SIMS analysis of pieces of single-crystal silicon that had been oxidized in the respective atmospheres: $n^*_{bg} = 0.0024$, $n^*_g = 0.96$. The increased ^{18}O isotope fraction in the equilibrating gas [above the normal isotope abundance of (0.002 05 ± 0.000 14)] is commonly observed for extremely high-purity oxygen.[52]

The oxygen isotope profiles in the $SrTiO_3$ samples were measured by means of time-of-flight secondary ion mass spectrometry (ToF-SIMS) on a ToF-SIMS IV machine (IONTOF GmbH, Münster, Germany), equipped with a high-energy Ga^+ gun for producing secondary ions for ToF analysis, a low-energy Cs^+ gun for sputter etching of the sample, and a low-energy electron flood gun for charge compensation. The Ga^+ gun was operated in burst mode, with an ion energy of 25 keV, an analysis raster of 100 μm × 100 μm, and a cycle time of 30 μs.[52] For each sample, two long depth profiles (up to 12 μm) and two short profiles (up to 150 nm) were acquired. The long profiles employed 2 keV Cs^+ ions, rastered over 300 μm × 300 μm at a beam current of approximately 150 nA; the short profiles employed 0.5 keV Cs^+, rastered over 300 μm × 300 μm at a beam current of approximately 30 nA. Charge compensation was accomplished with <20 eV electrons. The pressure in the main chamber of the SIMS machine was below 10^{-9} mbar during analysis. Negative secondary ions were detected. An example profile is shown in Fig. 2; the isotope diffusion profile is evident from both the $^{18}O^-$ and $^{18}O^{16}O^-$ signals.

The ^{18}O isotope fraction can be calculated either from O^- species or from O_2^- species according to procedures detailed elsewhere.[59] Similar values were obtained from both procedures, as is to be expected if the ToF-SIMS detector dead time is correctly taken into account. Crater depths were determined postanalysis with an NT1100 interference microscope (Veeco Instruments Inc., NY, USA). Values of $D^*(\infty)$, k^*_s, and Φ_0 were obtained by visual comparison of experimental isotope profiles with theoretical profiles computed numerically; the errors in these parameters correspond to the range of values which give good visual agreement between computed and experimental profiles. The first 1–2 nm of the isotope profiles were removed, as they correspond to the interfacial core.[59]

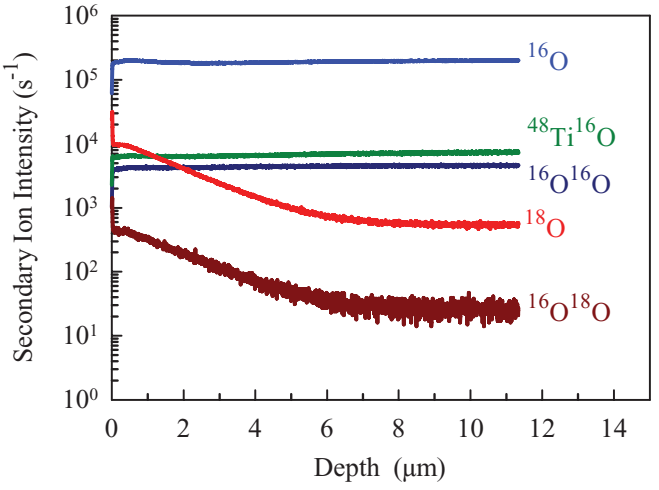

FIG. 2. (Color online) Secondary ion intensities against sputter depth obtained by ToF-SIMS depth profiling of an isotope exchanged $SrTiO_3$ substrate. Raw data corrected for the dead time of the detector.

IV. RESULTS

A. Near-surface structure and surface topography

In Fig. 3 we present a high-resolution transmission electron microscopy image obtained from the near-surface region of one of the samples used in the oxygen diffusion work, i.e., a nominally (100) oriented sample that had been subjected to a high-temperature pre-anneal, then the standard treatment in buffered HF, and finally, an $^{18}O/^{16}O$ anneal. The image shows that the entire region, extending from the original surface some 30 nm into the bulk, is composed solely of cubic perovskite lattice; neither SrO nor Ruddlesden-Popper phases $Sr_{n+1}Ti_nO_{3n+1}$ nor Magnéli phases Ti_nO_{2n-1} were observed.[68,69] The appearance of such phases is driven by an active partial SrO Schottky equilibrium [Eq. (3)], expelling SrO from $SrTiO_3$. The fact that no such phases were detected suggests that the equilibrium is kinetically hindered by low cation mobility.[61,62] Visual inspection of several bright-field TEM micrographs (not shown) failed to find a single dislocation in the (limited) volume of material investigated. This places an upper bound on the dislocation density of 10^8 cm^{-2}. For comparison the dislocation density in single-crystal $SrTiO_3$ has been measured to be 6×10^7 cm^{-2} in annealed specimens[70] and 6×10^9 cm^{-2} in polished but unannealed specimens.[71] Our results are thus consistent with a

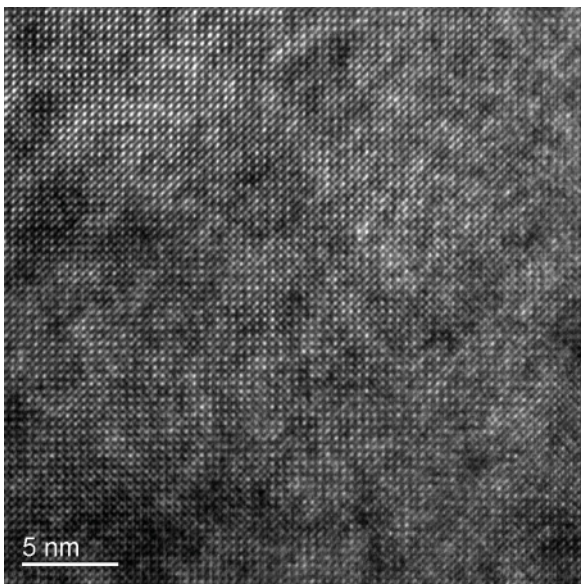

FIG. 3. HR-TEM micrograph of the surface region of a pre-annealed single crystal, showing only cubic perovskite lattice.

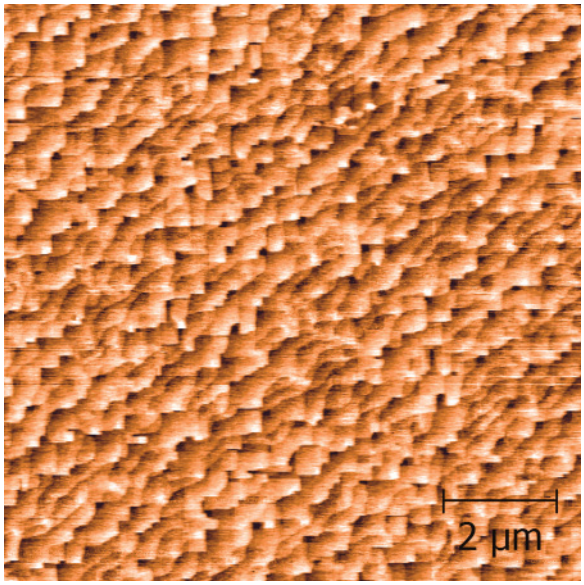

FIG. 4. (Color online) AFM micrograph of a nominally (100) oriented $SrTiO_3$ substrate subjected to a high-temperature pre-anneal, then the standard treatment in buffered HF, and finally, an $^{18}O/^{16}O$ anneal.

high-temperature pre-anneal yielding samples with diminished dislocation density.

Along ⟨100⟩ directions, an ABO_3 perovskite-type oxide consists of alternating AO and BO_2 planes. Consequently there are two possible terminations for a (100) surface: an AO plane or a BO_2 plane. In the case of $SrTiO_3$, domains of both terminations are commonly observed for a nominal (100) surface,[67,72] because the surface energies of the two terminations are rather similar.[73,74] The surface topography measured for the samples used in the oxygen diffusion work is shown in Fig. 4. A rather disordered surface structure is seen, and the step heights are multiples of 3.91 Å. In agreement with the TEM results, no evidence was found for SrO, $Sr_{n+1}Ti_nO_{3n+1}$, or Ti_nO_{2n-1}. Since buffered HF preferentially etches away SrO (Ref. 66) and the step heights correspond to multiples of $SrTiO_3$'s unit-cell parameter ($a = 3.905$ Å), this surface is evidently TiO_2 terminated. It is emphasized that all specimens treated according to the stated procedure exhibited this irregular surface structure, i.e., it is reproducible.

For completeness we also examined samples for which either the etching step or the high-temperature pre-anneal was left out. Samples that were not treated in buffered HF exhibited surface topography in which the step heights were half multiples of $SrTiO_3$'s unit-cell parameter, that is, the samples' surfaces have domains of both TiO_2 and SrO terminations. Preliminary oxygen isotope experiments on such samples indicated low amounts of isotope incorporated (see Fig. 5). On the other hand, samples that were not given a high-temperature pre-anneal prior to the treatment in buffered HF showed, as expected, the standard regular surface structure consisting of terraces that is characteristic of a vicinal (100) surface (see, e.g., Fig. 3 of Ref. 67). In preliminary oxygen isotope experiments on such samples, however, unusual and irreproducible features, which were attributed to the presence of polishing damage, were found in the measured isotope

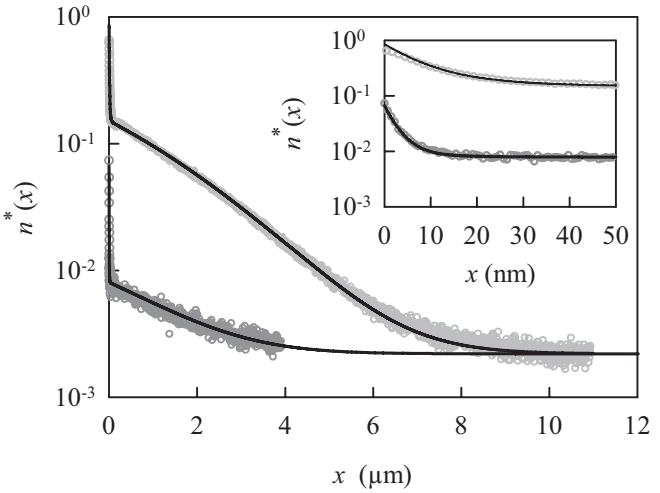

FIG. 5. Comparison of oxygen isotope diffusion profiles measured for $SrTiO_3$ single-crystal samples treated in buffered HF (light grey symbols) and not treated in buffered HF (dark grey symbols). Calculated solutions are shown as solid black lines. The inset shows the additional profile due to the space-charge layer. Both samples were exposed to ^{18}O-enriched gas at the same temperature ($T = 1123$ K) and oxygen activity ($aO_2 = 0.50$) for the same period of time ($t = 1.85 \times 10^3$ s).

profiles. Thus, whereas the high-temperature pre-annealing step prevents the regular terrace structure forming, it is evidently necessary to obtain reproducible isotope profiles.

B. Oxygen isotope diffusion

All isotope diffusion profiles measured for the single-crystal $SrTiO_3$ substrates displayed the same characteristic form: a sharp drop near the surface followed by an extended penetration profile into the material. The appearance of the additional isotope profile at the surface of these single-crystal samples unambiguously indicates the presence of an extended region of reduced diffusivity. We could assign this region of reduced diffusivity to an equilibrium space-charge layer that is depleted of (doubly) charged oxygen vacancies, first, and most importantly, because it is possible to describe (see Fig. 5) an entire isotope profile, from the surface, through the space-charge layer and into the bulk phase, with a single mathematical solution that contains only three fitting parameters [$D^*(\infty)$, k_s^*, and Φ_0]; and second, because the TEM results rule out alternative explanations, such as a layer of dislocations from polishing damage hindering diffusion or the presence of a second phase of lower diffusivity, formed by redistribution of SrO. It is also worth noting that no isotope profile exhibited a slowly decaying tail at large depths. Such features correspond to fast diffusion along dislocations[75,76] but are not expected here on account of the samples' low dislocation density.

Figure 5 compares oxygen isotope profiles obtained from two different samples, one treated in buffered HF to yield a TiO_2-terminated surface, and one not treated in buffered HF to maintain a mixed SrO/TiO_2-terminated surface. Both samples were exposed to ^{18}O-enriched gas at the same temperature and oxygen activity for the same period of time. For the

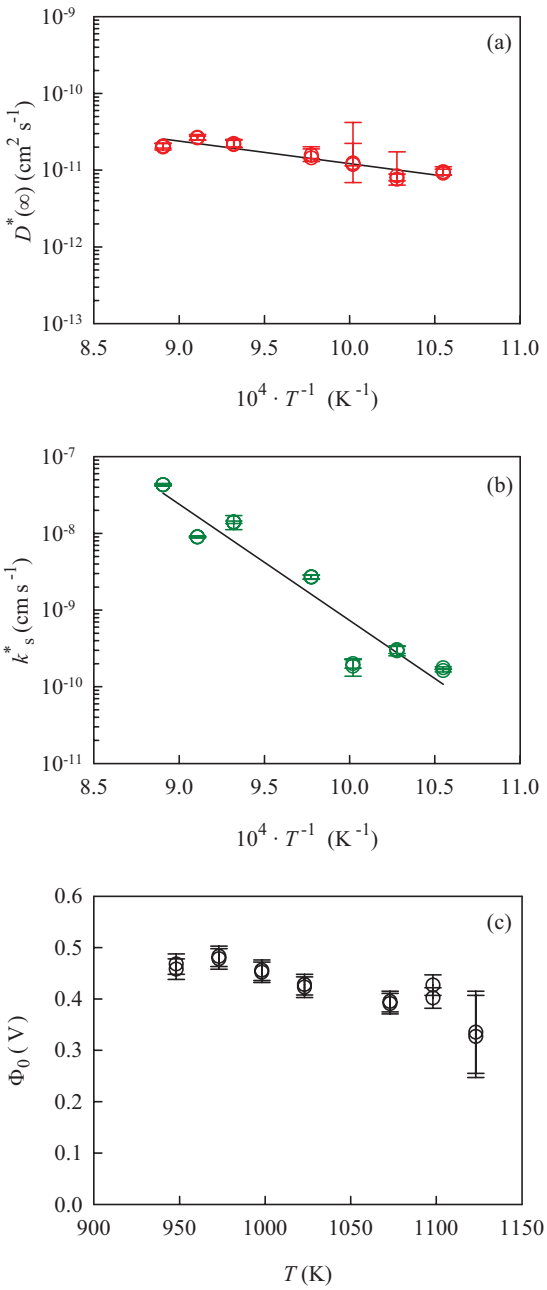

FIG. 6. (Color online) Temperature dependence at $aO_2 = 0.50$ of (a) the bulk tracer diffusion coefficient $D^*(\infty)$, (b) the surface exchange coefficient k_s^*, and (c) the surface space-charge potential Φ_0. The solid lines are fits to Arrhenius behavior.

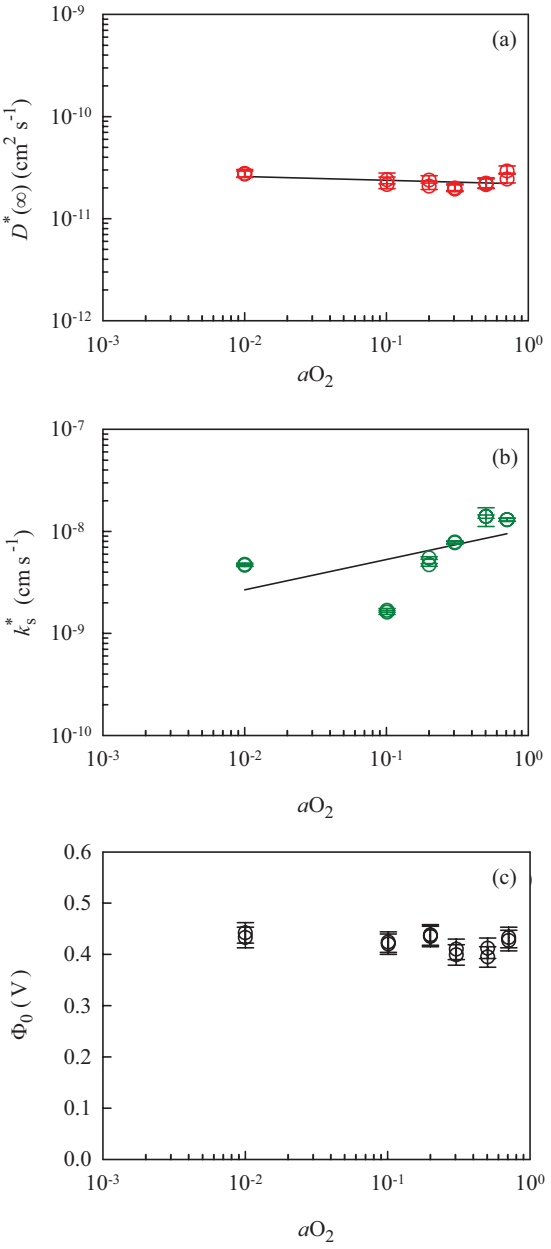

FIG. 7. (Color online) Oxygen activity dependence at $T = 1073$ K of (a) the bulk tracer diffusion coefficient $D^*(\infty)$, (b) the surface exchange coefficient k_s^*, and (c) the surface space-charge potential Φ_0. The solid lines are fits to power-law behavior.

etched sample, the experimental profile is best described with $D^*(\infty) = (2.1^{+0.3}_{-0.2}) \times 10^{-11}$ cm^2 s^{-1}, $k_s^* = (4.30^{+0.06}_{-0.06}) \times 10^{-8}$ cm s^{-1}, and $\Phi_0 = (0.33 \pm 0.08)$ V; the profile for the nonetched sample, with $D^*(\infty) = (1.4^{+1.4}_{-0.6}) \times 10^{-11}$ cm^2 s^{-1}, $k_s^* = (6.2^{+0.6}_{-0.6}) \times 10^{-10}$ cm s^{-1}, and $\Phi_0 = (0.43 \pm 0.01)$ V. Comparing bulk tracer diffusion coefficients, one finds that the values are similar: this is to be expected, since the bulk phase should not be affected by the etching of the surface. The precision, however, is greater for the etched sample because the degree of isotope enrichment is higher, $n^*(x)$ decreasing for the bulk profile by a factor of 75 to n^*_{bg} as opposed to a factor of 5 for the nonetched sample. As one of the aims of this study was to determine bulk diffusion coefficients with high precision, we used such HF-etched samples for all further diffusion experiments.

The drastic increase in the amount of incorporated isotope is due to k_s^* being two orders of magnitude higher and Φ_0 being possibly lower for the etched specimen. It is difficult to ascertain whether Φ_0 for the etched specimen is significantly lower because of the large uncertainty associated with this value (the additional isotope profile can be described equally poorly by a large range of Φ_0 values). Such a large uncertainty was only obtained for the sample subjected to the highest temperature exchange anneal. This may be due to strontium

vacancies starting to become mobile. The effect of surface treatment on k_s^* and Φ_0 is currently under investigation.

Tracer diffusion coefficients in the bulk $D^*(\infty)$, surface exchange coefficients $k_s{}^*$ and space-charge potentials Φ_0 obtained as a function of temperature T are summarized in Fig. 6 and as a function of oxygen activity aO_2 in Fig. 7.

V. DISCUSSION

A. Bulk diffusion

The bulk tracer diffusion coefficient $D^*(\infty)$ can be written as [see Eq. (11)]

$$D^*(\infty) = f^* D_V \frac{c_{V_O^{\cdot\cdot}}(\infty)}{c_{O_O^\times}(\infty)}. \quad (15)$$

In view of f^* being a constant (equal to 0.69 for an ABO_3 perovskite-type oxide),[77] D_V only being a function of temperature, and $c_{O_O^\times}(\infty)$ hardly varying with oxygen activity, the isothermal variation of $D^*(\infty)$ with oxygen activity indicates directly how the oxygen vacancy concentration varies with oxygen activity. Describing the behavior with a power law, $D^*(\infty) \propto (aO_2)^{m_{D^*(\infty)}}$, one finds that the power-law exponent is

$$m_{D^*(\infty)} = \left(\frac{\partial \ln D^*(\infty)}{\partial \ln aO_2}\right)_T = \left(\frac{\partial \ln c_{V_O^{\cdot\cdot}}(\infty)}{\partial \ln aO_2}\right)_T. \quad (16)$$

The data plotted in Fig. 7(a) yield $m_{D^*(\infty)} = (-0.037 \pm 0.026)$, where the error is the standard error in fitting a power law to the data. To a first approximation this value is zero. Thus it confirms unequivocally that these nominally undoped $SrTiO_3$ crystals are indeed acceptor doped: $c_{V_O^{\cdot\cdot}}(\infty)$ is independent of oxygen activity because it is fixed by the concentration of acceptor species [see Eq. (8)]. Taking the full charge neutrality condition that includes electronic defects [Eq. (7)], we predict, by defect chemical modeling with $c_{Acc'} = 7 \times 10^{17}$ cm^{-3} and numerical values of the equilibrium constants $K(T)$ taken from Shin *et al.*,[78] a value quantitatively consistent with experiment, $m_{D^*(\infty)} = -0.009$. If oxygen vacancies were generated solely by reduction [see Eq. (5)], that is, if the samples were not acceptor doped but undoped, one would expect a far stronger dependence, namely $m_{D^*(\infty)} = -0.167$. The corollary is that annealing such $SrTiO_3$ substrates in oxygen does not change the concentration of oxygen vacancies appreciably (though it does modify considerably the proportion of electron to holes).

The measured activation enthalpy of isotope diffusion is determined from the data in Fig. 6(a) to be $\Delta H_{D^*(\infty)} = (0.58 \pm 0.08)$ eV. Assuming that defect interactions are negligible, one can express $\Delta H_{D^*(\infty)}$ as the sum of the migration enthalpy of oxygen vacancies and the generation enthalpy of oxygen vacancies (the enthalpy change reflecting the variation in vacancy concentration with temperature),[79]

$$\begin{aligned}\Delta H_{D^*(\infty)} &= -\left(\frac{\partial \ln D^*(\infty)}{\partial(1/RT)}\right)_{aO_2} \\ &= -\left(\frac{\partial \ln D_V}{\partial(1/RT)}\right)_{aO_2} - \left(\frac{\partial \ln c_{V_O^{\cdot\cdot}}}{\partial(1/RT)}\right)_{aO_2} \\ &= \Delta H_{mig,V} + \Delta H_{gen,V}. \end{aligned} \quad (17)$$

TABLE I. Activation enthalpies for oxygen vacancy migration in $SrTiO_3$. C denotes a computational study.

Method	$\Delta H_{mig,V}$ (eV)	Ref.
Isotope diffusion	0.6	this study
Isotope exchange	1.13	23
Chemical diffusion	0.98	24
Chemical diffusion	0.3	26
Isotope exchange	1.06	28
Chemical diffusion	0.65	29
Chemical diffusion	2.1	31
Electrical conductivity	1.0	4
Nuclear-spin relaxation	0.62	32
Electrical conductivity	0.86	33
Anelastic relaxation	0.98	39
Anelastic relaxation	0.60	40
Electrical conductivity	1.4	41
Thermally stimulated relaxation	0.91	42
C: Empirical pair potentials	0.65	43
C: Empirical pair potentials	0.76	44
C: Density functional theory	0.4 – 0.7	45
C: Empirical pair potentials	0.9	46
C: Density functional theory	0.6	47
C: Density functional theory	0.6	48
C: Empirical pair potentials	0.96 – 1.35	49

Consequently if we assume Eq. (8) as the bulk charge neutrality condition, $c_{V_O^{\cdot\cdot}}(\infty)$ does not change with temperature (it is fixed by the concentration of acceptors), and therefore $\Delta H_{gen,V}$ is zero, and $\Delta H_{mig,V} = \Delta H_{D^*(\infty)} = (0.58 \pm 0.08)$ eV. If, once again, we extend the charge neutrality condition to include electronic defects [Eq. (7)], we predict, by defect chemical modeling, $\Delta H_{gen,V} = -0.04$ eV, and hence $\Delta H_{mig,V} = (0.62 \pm 0.08)$ eV. We therefore conclude that, regardless of which charge neutrality condition is used, the activation enthalpy for oxygen vacancy migration in $SrTiO_3$ is approximately 0.6 eV.

This value is in excellent agreement with oxygen-vacancy migration enthalpies determined for $SrTiO_3$ from macroscopic chemical diffusion measurements [(0.65 ± 0.06) eV],[29] and from microscopic investigations of vacancy hopping by means of nuclear-spin relaxation (0.62 eV),[32] and anelastic relaxation (0.6 eV).[40] The latest theoretical calculations based on density functional theory (DFT) also give a value of 0.6 eV.[47,48] Other experimental data[4,23,24,28,39,41] tend to cluster around 1 eV (see Table I), and we discuss possible reasons for this scatter below.

Absolute values of D_V extracted from the data in Fig. 6(a) with Eq. (15) are compared as a function of temperature in Fig. 8 with literature data for $SrTiO_3$.[4,24,26,29,31–33,41] Our values of D_V agree well with data from both macroscopic and microscopic methods: low-temperature conductivity,[4] chemical diffusion,[24,29] and nuclear-spin relaxation (NSR).[32] Hereby it should be noted that the NSR data[32] represent an upper limit, as D_V was calculated from the NSR correlation time τ_{NSR} according to $D_V = (4a^2 f_{NSR})/(6\tau_{NSR})$ assuming $f_{NSR} = 1$, whereas $f_{NSR} < 1$ is expected.[80] In addition, it is surprising that the data from Ref. 4 agree so well, given that

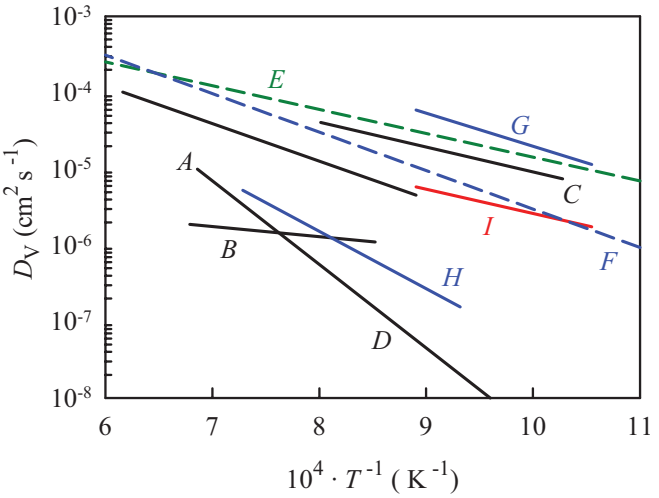

FIG. 8. (Color online) Comparison of oxygen vacancy diffusion coefficients in $SrTiO_3$ determined by various experimental methods. *A*: chemical diffusion (Ref. 24); *B*: chemical diffusion (Ref. 26); *C*: chemical diffusion (Ref. 29); *D*: chemical diffusion (Ref. 31); *E*: nuclear-spin relaxation (Ref. 32): *F*: electrical conductivity (Ref. 4); *G*: electrical conductivity (Ref. 33); *H*: electrical conductivity (Ref. 41); *I*: isotope diffusion (this study). Dashed lines are extrapolated from lower temperatures. Solid lines refer to the exact temperature interval investigated.

the data are extrapolated from much lower temperatures with a vacancy migration enthalpy of 1 eV. Bearing these points in mind, we obtain a global expression for the temperature regime, $948 > T/K > 1623$, that describes our data and the data from chemical diffusion measurements:[24,29]

$$\ln[D_V/\mathrm{cm}^2\,\mathrm{s}^{-1}] = -5.05^{+0.69}_{-0.77} - \frac{0.62\ \mathrm{eV}}{kT}. \qquad (18)$$

Alternatively, with the global expression

$$\ln[D_V/\mathrm{cm}^2\,\mathrm{s}^{-1}] = -4.96^{+0.45}_{-0.44} - \frac{0.67\ \mathrm{eV}}{kT}, \qquad (19)$$

we can describe our data, the data from Paladino's chemical diffusion measurements,[24] and two data points at much lower temperatures (473 and 573 K) derived from Blanc and Staebler's electrocoloration experiments.[27] Refining these global expressions further requires tracer diffusion data for $T < 950$ K. Due to low k_s^* values, however, catalytically active metal-oxide layers are necessary for sufficient ^{18}O to be incorporated into $SrTiO_3$.[35]

Last we return to the question of why is there so much scatter in the experimental values of D_V, and especially $\Delta H_{mig,V}$. We mention here three possibilities. One possible source of scatter arises from performing or evaluating a diffusion experiment incorrectly. The evaluation, for instance, will be incorrect if the wrong solution of Fick's second law is used to extract a diffusion coefficient: wrong because the boundary conditions employed in solving Fick's second law do not correspond to the experimental conditions.[52] Another source of erroneous values of D_V and thus $\Delta H_{mig,V}$ is incomplete or incorrect knowledge of the point defect chemistry of the actual samples investigated. As demonstrated here, calculating D_V from a measured diffusion coefficient (here, the isotope diffusion coefficient) requires quantitative knowledge of the samples' point defect chemistry, that is, one needs to know the type and concentration of acceptor dopants present. A third possibility is that the oxygen vacancy diffusion coefficient depends on the type of acceptor dopant, for example, because of association between oxygen vacancies and acceptor-dopant moieties. Al'_{Ti} appears not to bind vacancies at all in the temperature window investigated here (viz. we find no evidence for a significant binding energy), but Fe'_{Ti} and Ni''_{Ti} certainly bind vacancies at lower temperatures.[81] This may not only explain some scatter in reported migration enthalpies but also why they group around 1 eV.

VI. Surface space-charge layer

The space-charge potential is not a material-specific parameter. It is specific to a particular sample and a particular set of measurement conditions; it may thus exhibit rich behavior as a function of temperature, oxygen activity, and dopant concentration. Also, it only represents an intermediate, phenomenological level between measured properties and the fundamental thermodynamic driving energies for space-charge formation. It is these thermodynamic driving energies that are characteristic of the material system [e.g., $SrTiO_3$] and of the interface orientation and termination [e.g., a (100) TiO_2-terminated surface].[58]

A thermodynamic driving energy for space-charge formation for the defect building unit {def} (e.g., $\{V_O^{\cdot\cdot}\} = V_O^{\cdot\cdot} - O_O^{\times}$) is defined as the difference in the standard chemical potential of {def} in the interface core and in the bulk phase, $\Delta\mu^{\ominus}_{\{def\}} = \mu^{\ominus}_{\{def\}}(\mathrm{core}) - \mu^{\ominus}_{\{def\}}(\mathrm{bulk})$.[58,64,82–84] It is equivalent to the trapping energy of that defect at the interface.[58] Nonzero values of $\Delta\mu^{\ominus}_{\{def\}}$ force the redistribution of point defects between the interface core and the adjoining bulk phase. For example, in the case of a negative thermodynamic driving energy, $\Delta\mu^{\ominus}_{\{def\}} < 0$, the building unit {def} prefers to reside in the interface core. Given sufficient mobility, this building unit {def} will segregate to the interface core, electrically charging it in the process, and forming space-charge zones depleted of {def} in the adjacent bulk regions. The system has lowered its Gibbs free energy by redistributing defects between interface core and bulk phase. Equilibrium space-charge layers have formed when the electrochemical potentials of all mobile defects are constant throughout the system, $\nabla\tilde{\mu}_{\{def\}} = 0$. The electrochemical potential of building unit {def} in the bulk and in the interface core is assumed to take the form[58,64,85]

$$\tilde{\mu}_{\{def\}} = \mu^{\ominus}_{\{def\}} + RT\ln\frac{c_{\{def\}}}{N_{\{def\}} - c_{\{def\}}} + z_{\{def\}}e\phi. \qquad (20)$$

$N_{\{def\}}$ is the density of available sites. $N_{\{def\}}(\mathrm{core})$ is not necessarily equal to $N_{\{def\}}(\mathrm{bulk})$; it is generally some fraction thereof. In the following we assume a flat TiO_2-terminated surface and thus $N_{\{def\}}(\mathrm{core}) = N_{\{def\}}(\mathrm{bulk})$ for all mobile defects.

In this section the concern is the extraction of the relevant fundamental thermodynamic driving energies from experimental values of Φ_0. The sample is approximated as a continuum, as before (Sec. II B). It is considered to consist of an interfacial core phase of thickness w_c in contact with a bulk

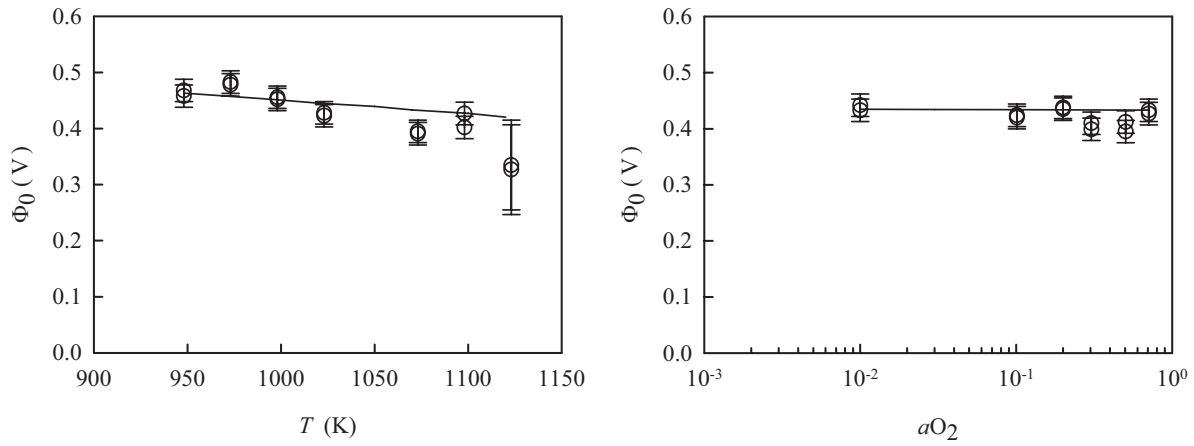

FIG. 9. Comparison of experimental data (open circles) and theoretical prediction (solid lines) for the surface space-charge potential Φ_0 (a) as a function of temperature T at $aO_2 = 0.50$, (b) as a function of oxygen activity aO_2 at $T = 1073$ K. Theoretical calculations assumed $\nabla\tilde{\mu}_{\{\text{def}\}} = 0$ for $\{\text{def}\} = V_O^{\cdot\cdot}, e', h^{\cdot}$, with $w_c = a/2$, $N_{\{\text{def}\}}(\text{core}) = N_{\{\text{def}\}}(\text{bulk})$ and $\Delta\mu^{\ominus}_{\{V_O^{\cdot\cdot}\}} = -1.42$ eV.

phase of infinite extent, with $\Delta\mu^{\ominus}_{\{\text{def}\}}$ changing abruptly across the junction.[58] The calculation of Φ_0 from a set of $\Delta\mu^{\ominus}_{\{\text{def}\}}$ requires, in addition to Eq. (20), that the sample as a whole is electrically neutral,[58,86]

$$\varepsilon_0\varepsilon_r \left.\frac{d\phi}{dx}\right|_{x=0} + w_c \sum z_{\{\text{def}\}} e[c_{\{\text{def}\}}(\text{core}) - c_{\{\text{def}\}}(\text{bulk})] = 0, \tag{21}$$

that is, the charge within the space-charge layer [obtained by integrating once the Poisson-Boltzmann equation, Eq. (10)] is exactly compensated by the charge of the surface core (due to the redistributed charged point defects). In the case of extended defects in acceptor-doped $SrTiO_3$ there are two possibilities that result in a positive space-charge potential, i.e., the formation of space-charge zones depleted of oxygen vacancies: $\Delta\mu^{\ominus}_{\{V_O^{\cdot\cdot}\}} < 0$, $\Delta\mu^{\ominus}_{\{h^{\cdot}\}} < 0$.[58] For the (100) TiO_2-terminated surface of $SrTiO_3$ theoretical calculations provide evidence for both: the valence-band edge is shifted up into the band gap by approximately 1 eV at the surface[73,87] and the formation energy of an oxygen vacancy is 1.5 eV lower at the surface.[88]

In Fig. 9 space-charge potentials predicted for $\Delta\mu^{\ominus}_{\{V_O^{\cdot\cdot}\}} = -1.42$ eV (with redistribution of oxygen vacancies, electrons, and electron holes allowed) are compared with those determined experimentally. It is seen that a single thermodynamic driving energy is able to describe the variation of Φ_0 with both temperature and oxygen activity. This provides additional evidence for the existence of an equilibrium space-charge layer at the surface of acceptor-doped $SrTiO_3$. Further calculations indicate that $\Delta\mu^{\ominus}_{\{h^{\cdot}\}}$ may take values up to -0.7 eV without influencing the predicted value of Φ_0. In other words, both $\Delta\mu^{\ominus}_{\{V_O^{\cdot\cdot}\}}$ and $\Delta\mu^{\ominus}_{\{h^{\cdot}\}}$ may be negative, but for this interface under these thermodynamic conditions, space-charge formation is driven by the former, the trapping of oxygen vacancies at the interface.

There is remarkably good agreement between the driving energy extracted from experiment and the value of -1.5 eV predicted from DFT calculations.[85] Theory, however, refers to neutral vacancies at an atomically flat TiO_2-terminated surface, whereas experiment refers to charged vacancies at a TiO_2-terminated surface with terrace edges and corners (see Fig. 4). We therefore consider it satisfactory to have extracted from experiment a thermodynamic driving energy for space-charge formation that has the appropriate order of magnitude.

A. Surface exchange

Several detailed studies have been devoted to investigating the surface reaction between gaseous oxygen and acceptor-doped $SrTiO_3$.[35,38,89–92] Nevertheless, the results obtained in this study are surprising in several respects. First, it is very surprising that etching away SrO-terminated regions increases k_s^* at $T = 1123$ K by almost two orders of magnitude. Evidently the TiO_2 termination exchanges oxygen faster than the SrO termination, as removing regions of the latter increases k_s^*. The area fraction of the active, TiO_2-terminated regions, however, increases perhaps by a factor of 5, and certainly not by two orders of magnitude, upon going from a mixed SrO/TiO_2 termination to a pure TiO_2 termination.[67,72] It appears that etching the (100) surface of $SrTiO_3$ with buffered HF alters more than just the termination.

The second surprising point is the large scatter in the data obtained—both as a function of temperature and as a function of oxygen activity—as evidenced by the large errors in the activation energy, $\Delta H_{k_s^*} = (3.01 \pm 0.28)$ eV, and in the power-law exponent, $m_{k_s^*} = (0.29 \pm 0.13)$, respectively. By using high quality single-crystal samples cut from a single boule and treated to yield the (100) TiO_2 termination, we aimed to produce surfaces of identical structure and composition. The large scatter strongly suggests that we did not achieve our aim, and the reason for this is unclear. Does the local surface structure (terrace edges and corners, surface reconstructions) or surface composition (segregated impurities/residual SrO) vary over a sample surface and between samples?

Third, there is surprisingly little difference between the activation energies for k_s^* and k_{eff}^* even though k_{eff}^* includes the effect of the space-charge potential. In this respect it is to be noted that $\Delta H_{k_{\text{eff}}^*} = (2.95 \pm 0.25)$ eV is comparable to those reported for Fe-doped $SrTiO_3$ single crystals (2.5–2.9 eV).[35]

Furthermore, the observed dependence of k^*_{eff} on oxygen activity, $m_{k^*_{\mathrm{eff}}} = 0.23 \pm 0.11$ is consistent with the empirical prediction[93] for a wide band-gap perovskite oxide doped with a fixed valence acceptor of $m_{k^*_{\mathrm{eff}}} = 0.25$.

Last we call for the results and conclusions of previous studies of the oxygen surface reaction on acceptor-doped $SrTiO_3$ to be re-examined.[35,38,89–92] In no study was the presence of the space-charge layer taken into account properly. In particular it needs to be recognized that the defect concentrations at the surface, that is, those that are relevant for the surface reaction, are not those in the bulk [Eq. (7)] but those in the surface core [Eq. (21)].[59]

VII. CONCLUSIONS

Oxygen vacancies govern diverse bulk and interfacial properties of the perovskite oxide $SrTiO_3$. Their behavior can be probed in oxygen diffusion experiments. Of the various types of diffusion experiment, the combination of isotope exchange and SIMS is the most time consuming and the most difficult to execute, but it is capable of delivering high quality, unambiguous diffusion data. In this study we have used isotope exchange experiments with ToF-SIMS analysis:

(1) to clarify the diffusion kinetics of oxygen vacancies in bulk $SrTiO_3$ and to derive a global expression to describe our data and selected literature data;

(2) to show that the oxygen vacancy concentration in nominally undoped $SrTiO_3$ single-crystal substrates is not altered significantly by annealing in oxygen owing to the samples being weakly doped with acceptor impurities;

(3) to demonstrate in detail that diffusion of a labeled isotope through a depletion space-charge layer can make the layer "visible" by giving rise to an additional isotope profile;

(4) to determine that space-charge formation at the (100) TiO_2-terminated surface of $SrTiO_3$ is driven by the preferential formation of oxygen vacancies at the surface.

ACKNOWLEDGMENTS

We gratefully acknowledge experimental assistance from and discussions with A. Rothschild, F. Gunkel, and R. Dittmann. AFM images were acquired by A. Aretz (GFE, RWTH Aachen University). The authors acknowledge funding by the DFG (German Science Foundation) within the collaborative research center SFB 917 "Nanoswitches."

*desouza@pc.rwth-aachen.de

[1] D. M. Smyth, Prog. Solid State Chem. **15**, 145 (1984).
[2] G. M. Choi and H. L. Tuller, J. Am. Ceram. Soc. **71**, 201 (1988).
[3] R. Waser, Ferroelectrics **133**, 109 (1989).
[4] R. Waser, J. Am. Ceram. Soc. **74**, 1934 (1991).
[5] I. Denk, W. Münch, and J. Maier, J. Am. Ceram. Soc. **78**, 3265 (1995).
[6] R. Moos and K.-H. Härdtl, J. Am. Ceram. Soc. **80**, 2549 (1997).
[7] R. A. De Souza, J. Fleig, R. Merkle, and J. Maier, Z. Metallkd. **94**, 218 (2003).
[8] R. Merkle and J. Maier, Angew. Chem. Intl. Ed. **47**, 3874 (2008).
[9] A. Ohtomo and H. Y. Hwang, Nature (London) **427**, 423 (2004).
[10] S. Thiel, G. Hammerl, A. Schmehl, C. W. Schneider, and J. Mannhart, Science **313**, 1942 (2006).
[11] M. Huijben, A. Brinkman, G. Koster, G. Rijnders, H. Hilgenkamp, and D. H. A. Blank, Adv. Mater. **21**, 1665 (2009).
[12] S. A. Chambers, M. H. Engelhard, V. Shutthanandan, Z. Zhu, T. C. Droubay, L. Qiao, P. V. Sushko, T. Feng, H. D. Lee, T. Gustafsson, E. Garfunkel, A. B. Shah, J.-M. Zuo, and Q. M. Ramasse, Surf. Sci. Rep. **65**, 317 (2010).
[13] S. Saraf, M. Markovich, and A. Rothschild, Phys. Rev. B **82**, 245208 (2010).
[14] K. Szot, W. Speier, G. Bihlmayer, and R. Waser, Nat. Mater. **5**, 312 (2006).
[15] R. Waser and M. Aono, Nat. Mater. **6**, 833 (2007).
[16] R. Waser, R. Dittmann, G. Staikov, and K. Szot, Adv. Mater. **21**, 2632 (2009).
[17] A. Kalabukhov, R. Gunnarsson, J. Börjesson, E. Olsson, T. Claeson, and D. Winkler, Phys. Rev. B **75**, 121404R (2007).
[18] W. Siemons, G. Koster, H. Yamamoto, W. A. Harrison, G. Lucovsky, T. H. Geballe, D. H. A. Blank, and M. R. Beasley, Phys. Rev. Lett. **98**, 196802 (2007).
[19] Y. Segal, J. H. Ngai, J. W. Reiner, F. J. Walker, and C. H. Ahn, Phys. Rev. B **80**, 241107R (2009).
[20] Y. B. Nian, J. Strozier, N. J. Wu, X. Chen, and A. Ignatiev, Phys. Rev. Lett. **98**, 146403 (2007).
[21] B. P. Andreasson, M. Janousch, U. Staub, G. I. Meijer, A. Ramar, J. Krbanjevic, and R. Schaeublin, J. Phys.: Conf. Ser. **190**, 012074 (2009).
[22] M. J. Rozenberg, M. J. Sánchez, R. Weht, C. Acha, F. Gomez-Marlasca, and P. Levy, Phys. Rev. B **81**, 115101 (2010).
[23] A. E. Paladino, L. G. Rubin, and J. S. Waugh, J. Phys. Chem. Solids **26**, 391 (1965).
[24] A. E. Paladino, J. Am. Ceram. Soc. **48**, 476 (1965).
[25] L. C. Walters and R. E. Grace, J. Phys. Chem. Solids **28**, 239 (1967).
[26] L. C. Walters and R. E. Grace, J. Phys. Chem. Solids **28**, 245 (1967).
[27] J. Blanc and D. L. Staebler, Phys. Rev. B **4**, 3548 (1971).
[28] A. Yamaji, J. Am. Ceram. Soc. **58**, 152 (1975).
[29] D. B. Schwarz and H. U. Anderson, J. Electrochem. Soc. **122**, 707 (1975).
[30] N.-H. Chan, R. K. Sharma, and D. M. Smyth, J. Electrochem. Soc. **128**, 1762 (1981).
[31] A. Müller and K.-H. Härdtl, Appl. Phys. A **49**, 75 (1989).
[32] A. Hackmann and O. Kanert, Radiat. Eff. Defects Solids **119–121**, 651 (1991).
[33] I. Denk, W. Münch, and J. Maier, J. Am. Ceram. Soc. **78**, 3265 (1995).
[34] J. Claus, M. Leonhardt, and J. Maier, J. Phys. Chem. Solids **61**, 1199 (2000).
[35] M. Leonhardt, R. A. De Souza, J. Claus, and J. Maier, J. Electrochem. Soc. **149**, J19 (2002).
[36] K. Szot, W. Speier, R. Carius, U. Zastrow, and W. Beyer, Phys. Rev. Lett. **88**, 075508 (2002).
[37] R. A. De Souza, J. Zehnpfenning, M. Martin, and J. Maier, Solid State Ionics **176**, 1465 (2005).

[38]C. Argirusis, S. Wagner, W. Menesklou, C. Warnke, T. Damjanovic, G. Borchardt, and E. Ivers-Tiffée, Phys. Chem. Chem. Phys. **7**, 3523 (2005).
[39]F. Cordero, A. Franco, V. R. Calderone, P. Nanni, and V. Buscaglia, Mater. Sci. Eng. A **442**, 55 (2006).
[40]F. Cordero, Phys. Rev. B **76**, 172106 (2007).
[41]C.-J. Shin and H.-I. Yoo, Solid State Ionics **178**, 1089 (2007).
[42]W. Liu and C. A. Randall, J. Am. Ceram. Soc. **91**, 3245 (2008)
[43]M. J. Akhtar, Z. Aktar, R. A. Jackson, and C. R. A. Catlow, J. Am. Ceram. Soc. **78**, 421 (1995).
[44]J. Crawford and P. Jacobs, J. Sol. State Chem. **144**, 423 (1999).
[45]J. Carrasco, F. Illas, N. Lopez, E. A. Kotomin, Yu. F. Zhukovskii, R. A. Evarestov, Yu. A. Mastrikov, S. Piskunov, and J. Maier, Phys. Rev. B **73**, 064106 (2006).
[46]B. S. Thomas, N. A. Marks, and B. D. Begg, Nucl. Instrum. Methods Phys. Res. B **254**, 211 (2007).
[47]D. D. Cuong, B. Lee, K. M. Choi, H.-S. Ahn, S. Han, and J. Lee, Phys. Rev. Lett. **98**, 115503 (2007).
[48]M. Lontsi-Fomena, A. Villesuzanne, J.-P. Doumerc, C. Frayret, and M. Pouchard, Comput. Mater. Sci. **44**, 53 (2008).
[49]C. R. A. Catlow, Z. X. Guo, M. Miskufova, S. A. Shevlin, A. G. H. Smith, A. A. Sokol, A. Walsh, D. J. Wilson, and S. M. Woodley, Philos. Trans. R. Soc. A **368**, 3379 (2010).
[50]J. A. Kilner and R. A. De Souza, in *Proceedings of the 17th Risø International Symposium on Materials Science, High Temperature Electrochemistry: Ceramics and Metals*, edited by F. W. Poulsen, N. Bonanos, S. Linderoth, M. Mogensen, and B. Zacharau-Christiansen (Risø National Laboratory, Roskilde, Denmark, 1996), p. 41.
[51]P. Fielitz and G. Borchardt, Solid State Ionics **144**, 71 (2001).
[52]R. A. De Souza and R. J. Chater, Solid State Ionics **176**, 1915 (2005).
[53]R. A. De Souza and M. Martin, Mater. Res. Soc. Bull. **34**, 907 (2009).
[54]J. A. Kilner, S. J. Skinner, and H. H. Brongersma, J. Solid State Electrochem. **15**, 861 (2011).
[55]R. Waser, Solid State Ionics **75**, 89 (1995).
[56]I. Denk, J. Claus, and J. Maier, J. Electrochem. Soc. **144**, 3526 (1997).
[57]R. Waser and R. Hagenbeck, Acta Mater. **48**, 797 (2000).
[58]R. A. De Souza, Phys. Chem. Chem. Phys. **11**, 9939 (2009).
[59]R. A. De Souza and M. Martin, Phys. Chem. Chem. Phys. **10**, 2356 (2008).
[60]R.-V. Wang and P. C. McIntyre, J. Appl. Phys. **97**, 023508 (2005).
[61]K. Gömann, G. Borchardt, A. Gunhold, W. Maus-Friedrichs, and H. Baumann, Phys. Chem. Chem. Phys. **6**, 3639 (2004).
[62]K. Gömann, G. Borchardt, M. Schulz, A. Gömann, W. Maus-Friedrichs, B. Lesage, O. Kaitasov, S. Hoffmann-Eifert, and T. Schneller, Phys. Chem. Chem. Phys. **7**, 2053 (2005).
[63]S. M. Sze, *Semiconductor Devices* (John Wiley & Sons, Ltd, New York, 1985).
[64]J. Maier, *Physical Chemistry of Ionic Materials* (John Wiley & Sons, Ltd., Chichester, 2004).
[65]J. C. Crank, *Mathematics of Diffusion*, 2nd ed. (Oxford University Press, New York, 1975), p. 36.
[66]M. Kawasaki, K. Takahashi, T. Maeda, R. Tsuchiya, M. Shinohara, O. Ishiyama, T. Yonezawa, M. Yoshimoto, and H. Koinuma, Science **266**, 1540 (1994).
[67]G. Koster, B. L. Kropman, G. J. H. M. Rijnders, D. H. A. Blank, and H. Rogalla, Appl. Phys. Lett. **73**, 2920 (1998).
[68]Y. Liang and D. Bonnell, J. Am. Ceram. Soc. **78**, 2633 (1995).
[69]K. Szot, W. Speier, J. Herion, and Ch. Freiburg, Appl. Phys. A **64**, 55 (1997).
[70]B. Stäuble-Pümpin, B. Ilge, V. C. Matijasevic, P. M. L. O. Scholte, and A. J. Tuinstra, Surf. Sci. **369**, 313 (1996).
[71]R. Wang, Y. Zhu, and S. M. Shapiro, Phys. Rev. Lett. **80**, 2370 (1998).
[72]N. Bickel, G. Schmidt, K. Heinz, and K. Müller, Phys. Rev. Lett. **62**, 2009 (1989).
[73]J. Padilla and D. Vanderbilt, Surf. Sci. **418**, 64 (1998).
[74]E. Heifets, R. I. Eglitis, E. A. Kotomin, J. Maier, and G. Borstel, Phys. Rev. B **64**, 235417 (2001).
[75]I. Kaur, Y. Mishin, and W. Gust, *Fundamentals of Grain and Interphase Boundary Diffusion* (John Wiley, Chichester, 1995).
[76]H. Mehrer, *Diffusion in Solids* (Springer-Verlag, Berlin, Heidelberg, 2007).
[77]T. Ishigaki, S. Yamauchi, K. Kishio, J. Mizusaki, and K. Fueki, J. Solid State Chem. **73**, 179 (1988).
[78]C.-J. Shin, H.-I. Yoo, and C.-E. Lee, Solid State Ionics **178**, 1081 (2007).
[79]R. A. De Souza and J. A. Kilner, Solid State Ionics **106**, 175 (1998).
[80]O. Kanert, Phys. Rep. **91**, 184 (1982).
[81]K. A. Müller, J. Phys. **42**, 551 (1981).
[82]D. M. Duffy and P. W. Tasker, Philos. Mag. A **50**, 155 (1984).
[83]J. Maier, J. Electrochem. Soc. **134**, 1524 (1987).
[84]J. Jamnik, J. Maier, and S. Pejovnik, Solid State Ionics **75**, 51 (1995).
[85]W. Göpel and H.-D. Wiemhöfer, *Statistische Thermodynamik* (Spektrum Verlag, Heildelberg, Berlin, 2000) (in German).
[86]P. McIntyre, J. Am. Ceram. Soc. **83**, 1129 (2000).
[87]E. Heifets, R. I. Eglitis, E. A. Kotomin, J. Maier, and G. Borstel, Surf. Sci. **513**, 211 (2002).
[88]J. Carrasco, F. Illas, N. Lopez, E. A. Kotomin, Yu. F. Zhukovskii, R. A. Evarestov, Yu. A. Mastrikov, S. Piskunov, and J. Maier, Phys. Rev. B **73**, 064106 (2006).
[89]Ch. Tragut and K.-H. Härdtl, Sens. Actuators B **4**, 425 (1991).
[90]T. Bieger, J. Maier, and R. Waser, Ber. Bunsenges. Phys. Chem. **97**, 1098 (1993).
[91]I. Denk, F. Noll, and J. Maier, J. Am. Ceram. Soc. **80**, 279 (1997).
[92]R. Merkle and J. Maier, Phys. Chem. Chem. Phys. **4**, 4140 (2002).
[93]R. A. De Souza, Phys. Chem. Chem. Phys. **8**, 890 (2006).